Liquid Crystals
Publication details, including instructions for authors and subscription information:
http://www.informaworld.com/smpp/title~content=t713926090

Crystal structure of 4-methoxybenzylidene-4'-*n*-butylaniline (MBBA) The C_4 and C_3 phases

M. More[a]; C. Gors[a]; P. Derollez[a]; J. Matavar[a]
[a] Laboratoire de Dynamique et Structure des Matériaux Moléculaires, (C.N.R.S. URA 801) U.S.T.L., Villeneuve d'Ascq Cedex, France

To cite this Article More, M. , Gors, C. , Derollez, P. and Matavar, J.(1995) 'Crystal structure of 4-methoxybenzylidene-4'-*n*-butylaniline (MBBA) The C_4 and C_3 phases', Liquid Crystals, 18: 2, 337 — 345
To link to this Article: DOI: 10.1080/02678299508036630
URL: http://dx.doi.org/10.1080/02678299508036630

LIQUID CRYSTALS, 1995, VOL. 18, NO. 2, 337–345

Crystal structure of 4-methoxybenzylidene-4′-*n*-butylaniline (MBBA) The C_4 and C_3 phases

by M. MORE*, C. GORS, P. DEROLLEZ and J. MATAVAR
Laboratoire de Dynamique et Structure des Matériaux Moléculaires, (C.N.R.S. URA 801) U.S.T.L., 59655 Villeneuve d'Ascq Cedex, France

(*Received 14 September 1993; in final form 20 May 1994; accepted 16 June 1994*)

Precise knowledge of thermal history (quenching and annealing) of the phases of the quenched liquid crystal MBBA has permitted us, from powder X-ray data, to attribute unequivocally a previously published structure to the C_4 metastable phase. Lattice parameters of the C_3 phase are also proposed.

1. Introduction

MBBA (4-methoxybenzylidene-4′-*n*-butylaniline) is a well-known thermotropic mesomorphic material which is considered as a model compound for liquid crystal studies [1, 2].

The elongated molecule has the formula

$$CH_3\text{–O–}\Phi\text{–CH=}N\text{–}\Phi\text{–}C_4H_9$$

where Φ is a phenyl group; it contains a central semi-rigid fragment and a more flexible alkyl chain which are both responsible for the formation of the mesophase. Near room temperature (between 19 and 36°C), MBBA forms a nematic phase, while on cooling, it exhibits a large variety of solid polymorphic modifications [3–6].

Rapid cooling ($\geqslant 40\ \mathrm{K\,min^{-1}}$) from the room temperature nematic phase yields an amorphous ground state called C_0, a glassy nematic-like liquid crystal with a glass transition temperature $T_g = 205$ K. Slow reheating of this C_0 glassy state leads to a variety of successive phases: C_1 and C_2 are relaxed disordered smectic-like structures, and C_3 and C_4 are crystalline phases [5]. The sequence C_0 to C_4 corresponds to a gradual molecular ordering occurring by transformations through different metastable stages. At a given temperature between T_g and room temperature, a given phase C_n evolves continuously with time towards the next C_{n+1} phase with a variable relaxation time. This is a reason why each transformation should be examined through a detailed study of its kinetics. Another reason is that the kinetics could provide information about the transformation mechanism.

Slow cooling from the room temperature phase (at a sufficiently moderated rate in order to prevent the quenching of the nematic phase), successively gives rise to the stable C_6 and then the C_5 crystalline phases [4].

The C_4 phase can transform to the nematic phase via a misunderstood mechanism (some authors report the existence of a plastic like state S [5]) and, a prolonged exposure of the C_6 phase nearly at the melting temperature would yield the C_4 phase after several tens of hours [7].

Figure 1 illustrates the phase diagram including all the previously described phases and the isotropic phase I.

X-ray diffraction measurements and studies of the kinetics of the transformations are a sure means of identifying the different structural modifications. We are now able to reproduce the sequence of phases, provided that the quenching and the various annealing processes are correctly performed.

No detailed structural information about all the different phases was known until a recently published X-ray study [8]. In this work, the authors were able to grow a monocrystal of MBBA on the goniometer head of an automatic diffractometer where they were using a miniature zone melting procedure with a focused IR laser beam to produce a local molten zone. They found a monoclinic structure, space group $P2_1$, $Z = 6$ with three independent molecules, and at 110 K: $a = 14{\cdot}908$ Å, $b = 8{\cdot}391$ Å, $c = 18{\cdot}411$ Å, $\beta = 96{\cdot}40°$. The molecular packing was smectic-like, with layers in the direction (001), the thickness of one layer being close to the c parameter of the unit cell. In view of the temperature of the experiment (110 K), the authors assigned the structure to the C_5 phase.

Using a simulation of this structure for a powder diffraction pattern (program PULVERIX [9]) and comparison with our powder measurements, we were able to show that the published data actually correspond to the C_4 structure.

Additional information is also given for the C_3 structure.

* Author for correspondence.

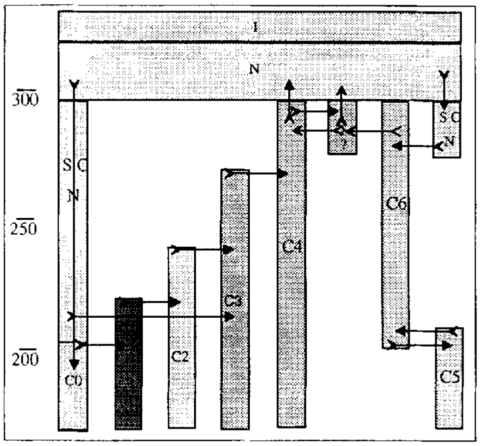

Figure 1. Symbolic phase diagram of MBBA at atmospheric pressure.

2. Experimental set-up

The sample, a viscous nematic fluid at room temperature, is inserted into a Lindemann glass capillary of diameter 0·7 mm and 5 to 8 mm long which can be continuously rotated around the vertical axis of a goniometer in order to average over all orientations perpendicular to the rotation axis.

The X-ray beam (CuK_{α}, 40 kV, 20 mA, $\lambda_{K_{\alpha}} = 1{\cdot}54059$ Å) is monochromatized by the $(10\bar{1}1)$ Bragg reflection of a curved quartz monochromator; its divergence is reduced by a set of vertical and horizontal slits which are also able to strip the K_{α_2} line.

Because of the complexity of the MBBA phase diagram and in order to perform a time-resolved data collection, the use of a position sensitive detector (PSD) was very helpful. The multidetector was of the gas flow type with a curved anode (INEL CPS120); the sample was in its centre. The X-ray photons scattered by the sample in the equatorial plane were measured over 120°, with an electronic resolution of about 0·03°, the window height being 8 mm. A beam stop allowed stripping of the incident beam. Electronic devices controlled the gas flux and pressure, and the high voltage, discrimination of the incoming pulses, allowing, through delay lines, the determination of the position and the intensity of the detected photons. Data were stored in a 4 K multichannel analyser providing a visualization facility and some possibilities for treatment. The diffraction patterns were then stored in a personal computer which was also used to pilot data collections. The instrumental width was about 5 channels (0·15°) FWHM with a nearly gaussian incoming beam shape.

The sample, centred on the axis of a vertical goniometer head, was introduced into a gas flow cryostat [10]. Cold gas (N_2 in our case) from a storage vessel was drawn through a flexible transfer tube and circulated through a heat exchanger using a gas flow pump. Thermal contact with the sample was achieved via helium gas exchange. The sample holder could be rotated from the top of the cryostat. Mylar windows enabled minimization of the attenuation of the incoming and scattered beams and their aperture allowed us to use the curved detector over all its angular range. The temperature was controlled to about 0·1 K. The cryostat was previously maintained at a temperature of about 100 K. To allow rapid quenching of the sample, the sample holder (at room temperature) was introduced into the cryostat chamber at 100 K; during the insertion, the temperature rose to 120 K only and we could anticipate a quenching rate of about 50 K s^{-1}.

In order to modify the effects of texture in the powder due to preferred alignment of the long molecules in the capillary, the room temperature nematic phase was first placed in an external magnetic field of about 1 Tesla outside the cryostat to align the molecules in a plane perpendicular to the capillary axis. After an alignment time of about 5 h, the sample was rapidly introduced into the cryostat. Comparison between patterns with and without preliminary application of the magnetic field showed that the number of observed Bragg peaks was generally higher when the molecules were previously aligned in this way.

All metastable phases were studied in the same way. After quenching of the oriented nematic phase at about 120 K, the sample was annealed for 10 h at 190 K. Then the temperature was increased until it was close to the C_0 to C_1 transition, for example. Because the kinetics of the transformation are faster when the temperature is closer to the temperature of the transition, data collections were repeated until the phase transition appeared and was complete. After a given transformation, the temperature was decreased to 110 K to stabilize the phase and a data collection was performed. All other transformations were made in the same way from the lowest temperature to room temperature in order to obtain the C_2, C_3 and C_4 phases according to the transformation temperatures indicated in figure 1.

Calibration of the detector with a powder sample of well-known lattice parameters allows non-linearities of the detector response [11] to be taken into account.

3. Results

3.1. *The C_4 phase*

The X-ray diffraction pattern of the 'oriented' C_4 phase registered at 110 K can be compared with the pattern simulated from the known structure using the PULVERIX program (see figure 2 (*a*), (*b*) and (*c*). (Comparison with the C_5 phase is also shown in figure 2 (*d*).) The measured and calculated peak positions for the C_4 phase are very similar considering the spectrometer resolution. Differences appear in the intensities: (i) the measured peaks at low indices have a lower intensity, probably due to the effect of orientation, (ii) the peaks with high indices in the

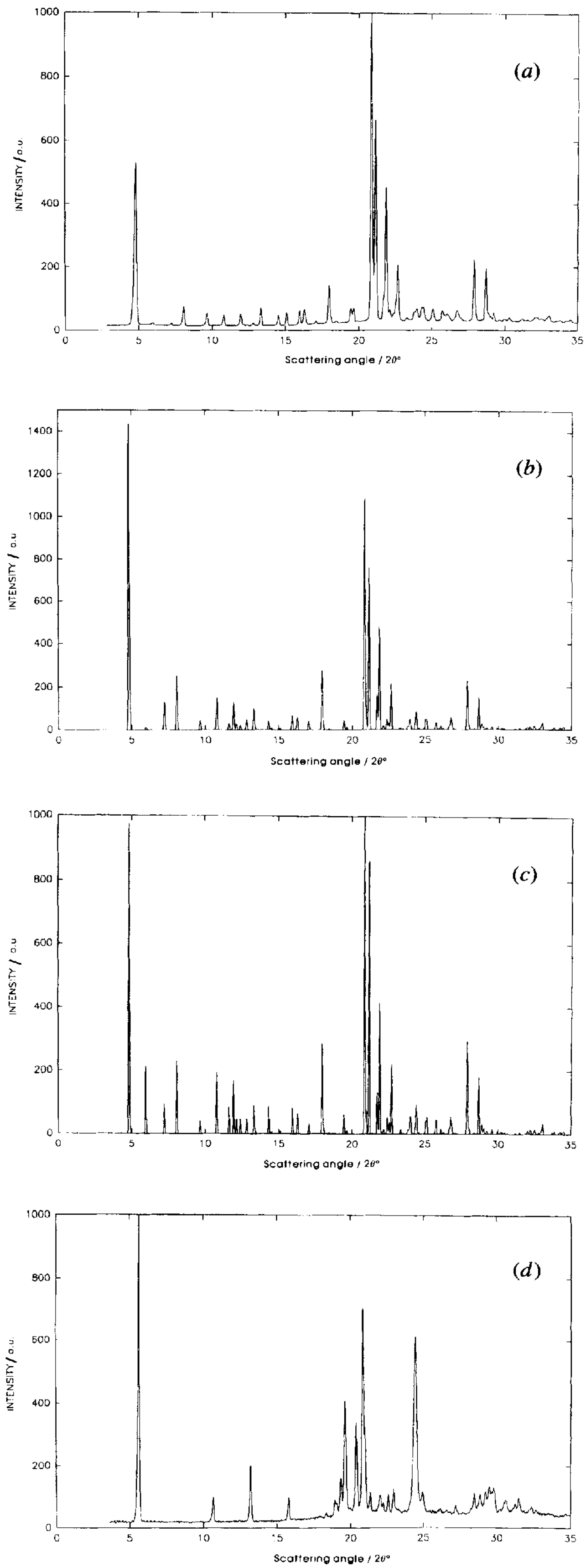

simulated powder pattern have greater intensities due to the fact that no correction is applied for the Debye–Waller factor. The positions of the peaks for the two patterns up to 50° are compared in table 1. They generally differ from each other from a maximum of 0·05°. Table 1 also shows the observed and calculated intensities. Results (Icalc 2) and (Icalc 1) (see table 1) correspond to calculation with and without hydrogen atoms, respectively. To take the hydrogen atoms into account, we have calculated their coordinates assuming that they are in standard positions. We can see that almost all the peaks with significant calculated intensities can be found in the observed data. A few exceptions are encountered: Bragg peaks (011), (201), (012), $(30\bar{1})$, $(31\bar{1})$, (122), $(40\bar{1})$, (412), $(32\bar{4})$, for example, are not observed, probably owing to the orientation effect. In table 1, all the calculated peaks are displayed in the 4° to 35° angular range. From 35° to 50°, only the peaks with intensities greater than 2·0 are noted in table 1, but, due to the lack of Debye–Waller corrections, calculated values are somewhat over-estimated. Table 2 reports the scattering angles and peak intensities for the C_5 phase for comparison.

A refinement of the cell parameters has been performed using the program DICVOL91 [12]. Table 3 shows the resulting cell parameters with 20, 30 and 50 peaks. De Wolff (M) [13] and Smith (F) [14] figures of merit are, respectively, [M(20) = 18·2, F(20) = 48·7], [M(30) = 14·8, F(30) = 51·1], [M(50) = 8·8, F(50) = 36·2].

Dynamical properties of the lattice vibrational modes of the C_4 phase have also been studied using Raman experiments and energy calculations. The program WMIN of BUSING [15] was used for this purpose. It consists in finding the minimum energy of molecular interactions from atom–atom potentials. For the calculation, we have chosen 6-exp potentials and have supposed that the molecules are rigid. Electrostatic interactions have not been taken into account. Hydrogen atoms with bond lengths of 1·08 Å are presumed to lie in the plane of the rigid phenyl groups, and for the aliphatic chains, to form approximately regular tetrahedra.

The values of the potential parameters are given by Williams [16, 17] (second column of table 4). Calculations were performed assuming that the interatomic vectors point into a sphere of 10 Å radius and the vectors of the

Figure 2. Comparison between observed (*a*) and calculated (*b*) and (*c*) X-ray powder diffraction patterns of the C_4 phase, and the observed pattern (*d*) of the C_5 phase in the range [0, 35] degrees in 2θ. Results of calculations (*b*) and (*c*) proceed from the PULVERIX program for the C_4 phase. In (*c*) the hydrogen atoms have been taken into account, while in (*b*) they have not. Intensities have been scaled to the (310) peak intensity.

Table 1. Comparison of the calculated and observed diffraction angles 2θ and intensities for the C_4 phase 2θ calc are the calculated angles from the known structure by program PULVERIX. 2θ obs are the observed angles from the powder diffraction data. I calc 1 are the calculated peaks intensities from the structure *without* the hydrogen atoms. I calc 2 are the same *with* the hydrogen atoms in standard positions. I obs are the observed intensities. The intensities are normalized to the intensity of the (310) peak.

hkl	2θ calc	2θ obs	I calc 1	I calc 2	I obs
001	4·83	4·82	1434	950·3	524
100	5·96	5·99	11·5	207·4	7·7
10-1	7·24	7·24	126·3	89·4	7·4
101	8·08	8·09	246	220·7	63·5
002	9·66	9·64	43	40·5	40
10-2	10·78	10·76	145	187·5	38·4
011	11·59		30	83·4	
102	11·91	11·92	120·5	147·9	38·4
200	11·94		1·4	19·2	
110	12·11	12·13	27·3	43·6	4·4
20-1	12·37	12·35	21·5	42·9	3·4
11-1	12·79	12·79	45·9	46·9	8·7
111	13·29	13·31	93·3	85·7	,61·6
201	13·37		11·5	9·9	
012	14·31		38·7	83·9	
003	14·51	14·53	5·7	4·7	31·6
20-2	14·52		1·4	0·6	
10-3	15·07		0·7	0·0	
11-2	15·09	15·09	6·2	8·5	40·2
112	15·93	15·98	50·2	63·1	45·9
210	15·95		14	17·6	
202	16·2		1	1·7	
21-1	16·28	16·31	54·5	59·7	48·8
103	16·31		1·4	1·1	
211	17·06	17·09	38·7	32·2	12·3
20-3	17·76		0·4	0·2	
300	17·95		15·8	37·4	
21-2	17·97	17·98	203	194·4	124·8
013	17·97		37·3	45·3	
30-1	18·06		12·9	14·4	
11-3	18·42	18·44	4·3	3·8	4·3
301	19·11		0·4	0·4	
212	19·36		1·7	1·3	
004	19·39		0	0	
30-2	19·44		14	21·9	
113	19·45	19·48	28·6	39·0	45·9
10-4	19·65	19·65	11·5	10·2	43
203	19·85	19·85	11·5	0·6	3
21-3	20·7		1·6	0·6	
310	20·85	20·89	1000	1000	1000
104	20·94		1·6	1	
31-1	20·95		73	66·6	
020	21·16	21·17	691	837·3	684·4
302	21·36		1·6	2·1	
20-4	21·65		0·3	0·2	
021	21·71	21·73	149	128·1	71·7
30-3	21·84		2·6	5·2	
311	21·87	21·89	433	391·5	441·9
120	22		0	5	
014	22·12	22·13	8·6	8·2	22·8
31-2	22·16		11·5	9·4	
11-4	22·34		1·4	1·7	
12-1	22·39	22·39	41·6	51·6	17·5
213	22·52	22·54	31·6	35·1	25·8
121	22·68	22·69	193·7	221·5	179·2
022	23·31	23·31	8·6	15·5	10·9
114	23·49	23·5	2·9	1·9	2·6
12-2	23·8	23·83	10	12	26·2
312	23·87		10	11·5	
40-1	23·96	23·99	34·4	36·7	36
204	23·96		0·7	0·5	
400	24·01		19·4	40·9	
21-4	24·13		2·2	1·3	
005	24·3	24·3	5·7	5·1	28·1
31-3	24·31		5·7	9·6	
122	24·35		15·8	19·5	
220	24·36		12·9	19·6	
10-5	24·38		4·4	1·7	
303	24·40	24·39	5·6	74·5	41·2
22-1	24·58		4·6	5·4	
40-2	24·89		0·7	0·6	
30-4	25		0·4	0·7	
40-1	25·04	25·09	35·8	39·2	37·7
221	25·11		38·7	52·2	
105	25·7		3·6	7·3	
22-2	25·75	25·75	22·4	33·7	33·1
023	25·75		5·7	8·5	
20-5	25·91	25·88	2·9	1·6	8·3
12-3	26·08	26·07	14·3	16·2	20·5
41-1	26·23		3·2	3·9	
214	26·23		0·3	0·8	
410	26·28		0·8	2	
015	26·55		1·6	1·7	
11-5	26·62		0·9	1·9	
313	26·65		12·9	15·1	
40-3	26·71		7	12	
222	26·76	26·76	43·7	48·1	32·4
123	26·83		20·5	22·2	
402	26·94	27·03	4·3	4·1	7·5
41-2	27·09		1·9	2·8	
31-4	27·19		0	0·1	
411	27·23		0·1	0·6	
22-3	27·76		2·3	2·3	
115	27·84		2	4·9	
320	27·88	27·92	199	284·1	196·6
32-1	27·96		11·8	9·7	
304	28		10	15·1	
21-5	28·04		1·4	2·8	
205	28·36		3·1	4·8	
321	28·66	28·71	132	177	158·4
30-5	28·67		2·7	2·3	
41-3	28·78		1·4	1·7	
024	28·85		10·2	14·4	
32-2	28·88	28·86	18	19·9	21·2
412	29		9·5	15·5	
12-4	29·03		2·4	4·1	
223	29·17		3	1·1	
10-6	29·21	29·24	3	7·4	23·8
40-4	29·26		2·6	2·9	
006	29·26		0·6	0·4	
403	29·56	29·63	12·8	15·2	5·2
124	29·94	29·99	3	7·4	8
50-1	29·98		0·7	0·8	
314	30·00		0·1	0·4	
500	30·14		2·4	7	

Table 1 (*continued*).

hkl	2θ calc	2θ obs	I calc 1	I calc 2	I obs
322	30·24		6·6	7·7	
215	30·33	30·31	2·3	1·4	12
20-6	30·4		3·3	3·9	
22-4	30·45	30·43	1·7	1·2	3·3
106	30·56		0	0·4	
32-3	30·59		0·7	1·5	
31-5	30·63	30·64	1·6	1·0	2·4
50-2	30·64		0·7	0·8	
501	31·08		0·1	0	
11-6	31·13		0·9	1·6	
41-4	31·18	31·19	3·3	2·6	8·6
016	31·18		0·3	0·1	
413	31·46	31·54	6·7	6·7	3·7
51-1	31·86	31·85	3·7	2·9	4·2
305	32·00		1·9	2·2	
510	32·01	32·06	5·9	7·3	12·9
50-3	32·05		4·6	5·1	
42-1	32·17		2·6	1·3	
224	32·17		7·5	11·6	
420	32·21	32·25	3·4	5·2	10·9
21-6	32·26		1	0·6	
031	32·35		0·4	1·3	
40-5	32·39		1	1·3	
116	32·41		1·1	1·7	
025	32·44		2	2·1	
51-2	32·48	32·51	11·6	10·9	10
12-5	32·50		0·8	1	
323	32·52		3·4	2·9	
130	32·55		1·6	2·2	
30-6	32·72		1·1	2·4	
404	32·74		0·4	0·8	
502	32·76		2·3	2·4	
13-1	32·82		2·1	2·4	
42-2	32·89		1·1	1	
511	32·91	32·86	5·6	4·5	7·6
206	32·96		3·4	2·1	
32-4	32·97		7·6	8·8	
421	33·00		3·9	3·5	
131	33·03	33·04	20·6	28·7	18·4
032	33·47		0·6	0·7	
125	33·52	32·52	0·1	0·1	6·2
22-5	33·69	33·62	4·3	4·8	2·4
315	33·78		0·7	0·4	
51-3	33·83		4·2	4·5	
13-2	33·83	33·83	5·5	5·3	6·2
10-7	34·13		0·1	0·1	
50-4	34·14		0·6	0·9	
41-5	34·15		2·6	3·6	
132	34·23		2·6	2·4	
230	34·24	34·27	5·2	4·7	6·6
007	34·28		1·6	2·5	
42-3	34·32		0·3	0·3	
23-1	34·4		7	6·8	
31-6	34·47		1·7	1·7	
414	34·48		8·9	7·5	8·5
422	34·50	34·53	0·1	0·1	
512	34·51		1·3	1·1	
216	34·7		0·9	0·7	
231	34·8		3·3	3·2	
20-7	35·08	35·08	3·9	4·7	6
503	35·09		1	1·2	
23-2	35·27	35·27	18	15·6	3·7
033	35·27		6·3	6·6	

hkl	2θ calc	2θ obs	I calc 1	I calc 2	I obs
324	35·36		4·7	5·9	
13-3	35·52		1·7	2·1	
11-7	35·82		0·6	1·5	
51-4	35·83	35·87	2·6	2·4	3·7
32-5	35·91		4	4·5	
232	36·04		9·5	10	12·6
133	36·09	36·07	13·8	13·3	
12-6	36·35		1·9	0·9	
600	36·35		0	1·7	
405	36·36	36·37	0·6	0·2	2·7
42-4	36·39		0·6	0·5	
026	36·39		2·4	2·9	
423	36·63		10·3	10·4	
513	36·73	36·71	3·6	5	
23-3	36·81		18	19·3	15·3
330	36·9	36·89	33·7	37·3	32·8
33-1	36·96		5·9	8·2	
126	37·47		6·4	6·5	
331	37·52	37·50	40·7	48·1	20·8
52-2	37·53		5·9	6	
034	37·67		0·9	0·9	
33-2	37·69	37·66	12	10·4	17·6
60-3	37·72		5·2	5·5	
316	37·88		4	5·6	
521	37·91		2·1	3·6	
233	37·91	37·91	8·3	11·1	8·3
504	37·95		1	0·4	
610	37·95		1·4	0·3	
415	37·95		6·4	7·3	
611	38·82	38·82	13·9	13·2	7·9
23-4	38·94		2·7	2	
42-5	39·02		7·5	4·9	
32-6	39·3		1·3	2·8	
424	39·31	39·31	5·2	5·7	4·2
514	39·49	39·45	6·4	9·6	8·5
226	39·50		3·3	2·4	
20-8	39·9	39·85	8·6	12·6	20
234	40·34		4·3	3·7	
612	40·3	40·31	6·3	5·8	7·9
52-4	40·52	40·55	8·5	8·9	5·3
603	40·9	40·93	4·6	5	6·2
43-2	40·94		1·9	2·4	
431	41·03		4·7	5	
523	41·33	41·31	5	6	4·9
416	41·79		4·4	4·8	
118	42·01	42·04	3·6	4·4	3·4
317	42·24		2·6	2·3	
62-1	42·25	42·23	4·6	4·1	1·9
613	42·35	42·37	5·4	4·6	2·7
425	42·44		3·7	4·2	
208	42·62		1·6	2·1	
62-2	42·65	42·59	3·7	5·3	1·3
31-8	43·07	42·96	5·3	5·7	5·3
61-5	43·18	43·18	10·2	11	7·6
621	43·24		13·5	16·7	
041	43·38		7·2	5·8	
33-5	43·48		3·9	5·3	
218	44·03		0·6	0·6	
40-8	44·12	44·03	9·9	11·9	10·8
10-9	44·25	44·21	5·3	5·4	9·6
60-6	44·53		0·3	0·1	
009	44·53	44·51	11·6	14·7	18·7
14-2	44·54		9	8·3	

Table 1 (*continued*).

hkl	2θ calc	2θ obs	I calc 1	I calc 2	I obs
53-2	44·87	44·87	5·3	6·4	12·3
22-8	45·60		10·5	10·8	
11-9	45·62	45·63	9·2	12·1	22·1
52-6	45·65		1	0·6	
109	45·68		8·2	8·5	
24-2	45·70		3·4	2·8	
14-3	45·9		2·9	3·1	
21-9	46·22	46·27	3	3·2	5·2
143	46·36		3·9	3·8	
327	46·39		4	4·9	
434	46·41		4·3	4·4	
71-4	46·46	46·46	7	6·7	7·5
623	46·49		8·3	10·6	
340	47·02	47·07	10·3	12·8	6·3
34-1	47·07		3·6	3·1	
341	47·53		8	8·5	
31-9	47·65	47·64	8·6	9·9	8·5
34-2	47·67		3	3·8	
720	48·11		3·1	4·6	
713	48·25	48·26	3·8	4·3	6·3
144	48·37		4·9	4·7	
342	48·57		8·6	8·1	
51-8	48·69	48·64	2·3	1·7	3·6
63-1	49·01		2·1	2·1	
630	49·18	49·24	2·4	1·9	1
42-8	49·43	49·41	3·1	2·9	0·7
029	49·8		6·2	7·6	
631	49·89		18·5	18·8	
440	49·92		3	2·3	

Table 2. Scattering angles and observed intensities for the C_5 phase.

2θ obs	I obs	2θ obs	I obs
5·73	1000	23·3	8
10·65	81	23·75	7
13·21	183	24·44	541
15·8	73	24·93	52
18·36	17	27·21	22
18·94	46	28·46	52·2
19·07	33	28·86	46·2
19·34	114	29·22	61·3
19·62	333	29·49	77·9
20·39	266	29·79	74·5
20·84	641	30·59	31·8
20·99	236	31·25	19·2
21·36	54	31·51	42
22·02	52	32·35	14·7
22·24	28	34·66	4·7
22·59	56	34·9	4·2
22·95	76	35·8	9·5
23·12	11	36·16	13·8

Table 3. Cell parameters for the C_4 phase from the 'DICVOL91' refinements versus the number of peaks taken into account, and the related figures of merit M and F.

N peaks	*a*/Å	*b*/Å	*c*/Å	β/°	*M*	*F*
20	14·897 (0·014)	8·376 (0·008)	18·409 (0·013)	96·56 (0·09)	18·2	48·7
30	14·891 (0·009)	8·386 (0·003)	18·411 (0·007)	96·51 (0·04)	14·8	51·1
50	14·872 (0·007)	8·388 (0·002)	18·415 (0·007)	96·5 (0·03)	8·2	36·2

Table 4. Initial and final potential parameters for the C_4 phase from a 'WMIN' refinement. (van der Waals): $E^{W}_{jk} = -A_{jk}/r^{6}_{jk}$; (repulsion): $E^{R}_{jk} = B_{jk}\exp(-C_{jk}r_{jk})$.

	Initial parameters	Final parameters	Relative variations/10^{-2}
$A_{C\text{-}C}$/kcal Å^6 mol^{-1}	583·13	577·29	1·0
$A_{O\text{-}O}$	268·55	285·18	6·2
$A_{N\text{-}N}$	329·45	389·74	18·3
$A_{H\text{-}H}$	32·60	32·90	0·9
$B_{C\text{-}C}$/kcal mol^{-1}	88370·7	88107·1	0·3
$B_{O\text{-}O}$	54986·6	56640·2	3·0
$B_{N\text{-}N}$	60833·9	66392·3	9·1
$B_{H\text{-}H}$	2861·1	2875·1	0·5
$C_{C\text{-}C}$Å^{-1}	3·60		
$C_{O\text{-}O}$	3·96		
$C_{N\text{-}N}$	3·78		
C_{H+NH}	3·74		

reciprocal lattice into a sphere of 0·3 Å^{-1} radius. At the convergence, the lattice parameters a, b, and c have been respectively changed by 2·3, 1·4, and 0·9 per cent and the monoclinic angle by −1·1 per cent. The molecular centres of mass are translated by no more than 0·1 Å and the molecular rotations are less than 2°. These results are relatively satisfactory for such a phase. The calculated energies are $E^W = -48{\cdot}2$ kcal mol^{-1} and $E^R = 19{\cdot}0$ kcal mol^{-1} giving a total lattice energy $E^T = -29{\cdot}2$ kcal mol^{-1}.

We have also tested the potential parameters from a refinement of the A_{jj} and the B_{jj} coefficients. The C_{jj} parameters have been kept fixed because of their dependence on the B_{jj} parameters. The final values of the parameters and their related variations are displayed in table 4. The carbon and hydrogen parameters vary less than the oxygen and nitrogen parameters. This is probably due to the fact that the coulombic interactions have been neglected. Nevertheless, there are only one oxygen and one nitrogen atom in the 41 atoms of the molecule and we can suppose that their contribution to the total potential is negligible. This is shown by the minimum final energy −29·3 kcal mol^{-1} which is close to that obtained with the starting parameters (−29·2 kcal mol^{-1}).

The measured Raman frequencies (see figure 3) for the C_4 phase are compared with the calculated values in table 5. We can obtain 33 optical modes which are all Raman active, but many of them are not experimentally resolved (see figure 3).

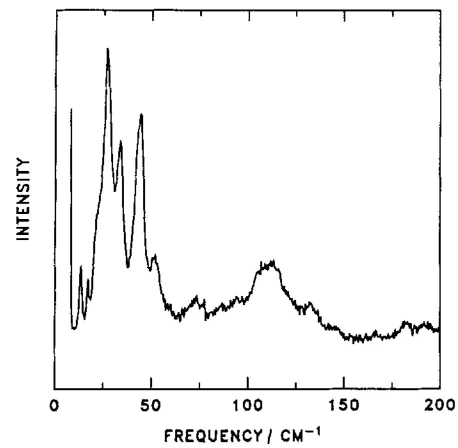

Figure 3. Raman spectrum of the C_4 phase.

3.2. *The C_3 phase*

Annealing of the C_0 phase at 240 K gives the C_3 phase. When the transformation is completed, a further annealing at 270 K produces the C_4 phase. The structure of the C_3 phase not being directly correlated with the C_4 phase, the structure does not appear obvious owing to the texture of the sample.

The collected data for the C_3 phase at 110 K have been used to define the cell parameters. From the powder diffraction pattern shown in figure 4, the first 23 peaks have been used with the program DICVOL91. We have obtained a monoclinic cell with parameters: $a = 14{\cdot}119(0{\cdot}010)$ Å, $b = 6{\cdot}763(0{\cdot}006)$ Å, $c = 16{\cdot}067(0{\cdot}009)$ Å, $\beta = 100{\cdot}83(0{\cdot}06)°$ which corresponds to a volume of $V = 1506{\cdot}9$ Å^3. The figures of merit are: M(23) = 6·5, F(23) = 12·0. The volume of the C_4 phase being 2282·2 Å^3 with $Z = 6$, the cell of the C_3 phase contains four molecules ($Z = 4$, $V = 1521$ Å^3). Table 6 gives the indices and the intensities of the observed Bragg peaks.

Table 5. Calculated (Calc) and observed (Exp) Raman frequencies for the C_4 phase and experimental values of half width at half maximum (HWHM).

Exp/cm^{-1}	Exp HWHM/cm^{-1}	Calc/cm^{-1}	Exp/cm^{-1}	Exp HWHM/cm^{-1}	Calc/cm^{-1}
13·2	1·6				67·5–67·6
16·8	1·4				69·4
		19·9	73·1	15	75·4–76·7
21·9	4·1				78·5–78·8
		24·6			83·3
27·2	5·3				87·7
		29·2	92·1	18·3	94·2
33·6	4·6	33·1–33·4			96
		38·2			98·1
42·4	5·2	43·3			100·3
44·5	4·1	45·5–46·6	106·1	9·7	104·8
		48·2			109
52·2	6·4	52·4–53·1	114·7	13·6	113·8
		55·1			116·3
59·4	8·4	59·6	132·9	19·6	
		62·2–62·4			

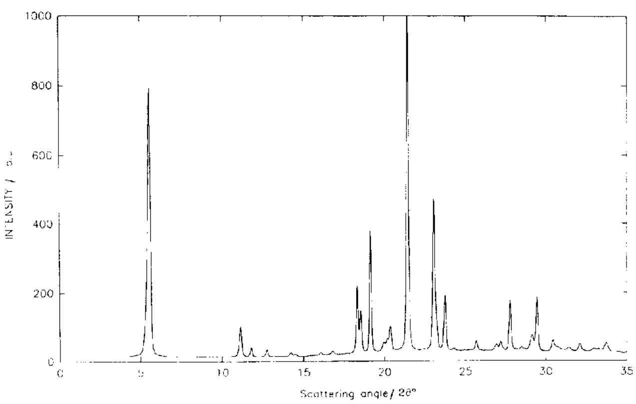

Figure 4. X-ray powder diffraction pattern of the C_3 phase.

4. Conclusions

We are able to show that the C_4 phase of MBBA corresponds to the structure that had been previously determined by Boese *et al.* [8], and wrongly attributed to the C_5 phase. This result has been obtained by comparing the results from our powder diffraction studies with a simulated pattern given by this structure. This has been achieved by a precise knowledge of thermal treatments and particularly by the ability, using a multidetector, to follow the progress of the transformations kinetics. It is obvious that the procedure employed (in [8]) to grow the monocrystal has been done in such a way that the quenched C_0 phase has been obtained first and then transformed to the 'more stable' C_4 phase by annealing. It remains for the structure of the C_5 and C_6 phases to be determined. These phases have been modelled: (i) from results of energy calculations using atom–atom potentials from series of mesomorphic fluorinated derivatives [18, 19] and (ii) from a structure based on that of EBBA [4]. Simulations of powder diagrams of these structures do not coincide with our powder results, and it would be helpful to perform other measurements using the method employed to grow low temperature monocrystals. It seems that this could be achieved by first, growing the C_6 phase at a temperature near the nematic to C_6 transformation, and then lowering the temperature to the C_5 phase, since this transition appears to be nearly second order.

Table 6. Observed (2θ obs) and calculated (2θ calc) diffraction angles for the C_3 from the DICVOL91 program and the corresponding observed intensities.

hkl	2θ calc	2θ obs	I obs	hkl	2θ calc	2θ obs	I obs
001	5·59	5·56	780·6	41-1	28·51	28·51	7·5
002	11·2	11·14	90·7	41-2	29·24	29·15	44·5
10-2	11·81	11·79	26·2	22-1	29·44	29·45	165·5
200	12·76	12·75	19·7	221	30·38		
011	14·24	14·23	11·2	411	30·41	30·44	26·5
110	14·56	14·49	5·9	22-2	30·61	30·69	13·3
111	16·04	16·05	7·4	023	31·42	31·42	11·1
003	16·84	16·78	10·9	12-3	31·43		
10-3	16·85			50-2	32·11	32·11	21·8
210	18·31	18·31	200·1	412	32·87	32·95	6·5
202	18·54	18·52	123·7	205	33·3	33·25	9·1
103	19·12			41-4	33·73	33·74	27·3
112	19·14	19·13	366·5	51-1	34·39	34·26	2·9
20-3	19·15			510	34·94	34·99	1·3
211	19·86	19·96	24·6	32-3	35·3	35·37	11·6
21-2	20·21	20·17	32·6	502	36·26	36·21	3·6
30-2	20·34	20·36	75·7	016	36·63		
013	21·39			21-6	36·65	36·66	2·4
11-3	21·39	21·44	1000	420	37·11	37·02	6
30-3	23·09	23·05	456	305	37·37		
113	23·24	23·23	71·8	42-2	37·37	37·41	5·4
20-4	23·74	23·73	164·9			37·73	2·8
31-2	24·26	24·27	7·4	60-1	38·25	38·23	14·9
400	25·68	25·67	28·4	206	38·80		
021	26·94	26·91	17·7	42-3	38·83	38·82	16·01
120	27·12	27·19	24·9	224	28·83		
10-5	27·76	27·78	153·5	60-3	39·5	39·5	39·7
114	27·93			130	40·51	40·54	10·8
121	27·96			61-1	40·59		
303	27·96	27·98	3·1	61-2	40·78	40·85	3·5
				11-7	41·53	41·53	8·2

References

[1] CHANDRASEKHAR, S., *Liquid Crystals* (Cambridge University Press), p. 342.

[2] DE JEU, W. H., 1980, *Physical Properties of Liquid Crystalline Materials* (Gordon & Breach), p. 133.

[3] DOLGANOV, V. K., KROO, N., ROSTA, L., SHEKA, E. F., and SZABON, J., 1985, *Molec. Crystals liq. Crystals*, **127,** 187.

[4] ROSTA, L., KROO, N., DOLGANOV, V. K., PACHER, P., SIMKIN, V. G., TÖRÖK, GY., and PEPY, G., 1987, *Molec. Crystals liq. Crystals*, **144,** 297.

[5] PEPY, G., FOURET, R., MORE, M., and ROSTA, L., 1989, *Physica Scripta*, **39,** 485.

[6] FOURET, R., ELOUATIB, A., GORS, C., MORE, M., PEPY, G., and ROSTA, L., 1991, *Phase Transit.*, **33,** 209.

[7] BELUSKIN, A. V., DOLGANOV, V. K., NATKANIEC, I., and SIMKIN, V. G., 1987, *Molec. Crystals liq. Crystals*, **15,** 187.

[8] BOESE, R., ANTIPIN, M. YU., NUSSBAUMER, M., and BLÄSER, D., 1992, *Liq. Crystals*, **12,** 431.

[9] YVON, K., JEITSCHKO, W., and PARTHE, E., 1977, *J. appl. Crystallogr.*, **10,** 73.

[10] ODOU, G., and NAVIEZ, D., 1987, *Spectra 2000*, No. 137, Vol. 17.

[11] EVAIN, M., DENIARD, P., JOUNNEAUX, A., and BREC, R., 1993, *J. appl. Crystallogr.*, **26,** 563.

[12] BOULTIF, A., and LOUËR, D., 1991, *J. appl. Crystallogr.*, **24,** 987.

[13] DE WOLFF, P. M., 1968, *J. appl. Crystallogr.*, **5,** 108.

[14] SMITH, G. S., and SNYDER, R. L., 1979, *J. appl. Crystallogr.*, **12,** 60.

[15] BUSING, W. R., 1981, *Acta crystallogr.* A, **28,** 252.

[16] WILLIAMS, D. E., and HOUPT, D. J., 1986, *Acta crystallogr.* B, **42,** 28.

[17] WILLIAMS, D. E., and COX, S. R., 1984, *Acta crystallogr*, B, **40,** 404.

[18] SEREDA, S. V., TIMOFEEVA, T. V., ANTIPIN, M. YU., and STRUCHKOV, YU. T., 1992, *Liq. Crystals*, **11,** 839.

[19] SEREDA, S. V., TIMOFEEVA, T. V., and STRUCHKOV, YU. T., 1991, *Soviet Phys. Crystallogr.*, **36,** 446.